# A SYNOPTIC-CLIMATOLOGY OF NORTHERN HEMISPHERE POLAR AND SUBTROPICAL JET SUPERPOSITION EVENTS

*by*

CROIX E. CHRISTENSON and JONATHAN E. MARTIN

*Department of Atmospheric and Oceanic Sciences*
*University of Wisconsin-Madison*
*1225 W. Dayton Street*
*Madison, WI 53705*
*jemarti1@wisc.edu*

Submitted for publication in *Journal of Climate*:
4 March 2014

# ABSTRACT

Narrow, tropopause-level wind speed maxima known as jet streams or jets are among the most ubiquitous structural characteristics of the Earth's atmosphere. Two jet species can be observed on any given day. The polar jet is tied, via the thermal wind relationship, to the troposphere-deep baroclinicity of the middle latitudes while the subtropical jet is tied, by angular momentum constraints, to the poleward edge of the tropical Hadley Cell. As a consequence of their different origins, the polar and subtropical jets are separated by both latitude and elevation. However, there are times when these two usually separate features become vertically superposed to form a single, intense jet core designated as a jet superposition.

An objective method for identifying tropopause-level jets is employed in the construction of 51-yr synoptic-climatologies of the Northern Hemisphere polar jet, subtropical jet, and jet superposition frequencies. The analysis demonstrates that while superposition events are relatively rare, there are clear geographical and seasonal maxima. Superpositions are most frequent in the western Pacific from December through February, abruptly decreasing in late winter (March/April), then increasing substantially again in late autumn (October/November). Consistent with expectations, the spatiotemporal maxima in jet superpositions appear to be coincident with maxima in the polar and subtropical jets.

## 1. Introduction

Narrow, rapidly flowing currents of air located near the tropopause are known as jet streams or jets. These jets, often found nearly girdling the globe while exhibiting large meridional meanders, are among the most ubiquitous structural characteristics of the Earth's atmosphere and are known to play a substantial role in the production of sensible weather in the mid-latitudes. Prior observational work has identified three major jet features; the subtropical jet, the polar jet, and the Arctic jet. The subtropical jet is located at the poleward edge of the Hadley cell (~30° latitude) in the tropical/subtropical upper troposphere (~ 200 hPa) (Loewe and Radok 1950, Yeh 1950, Koteswaram 1953, Mohri 1953, Koteswarma and Parthasarathy 1954; Sutcliffe and Bannon 1954, Defant and Taba 1957, Krishnamurti 1961, Riehl 1962) while the polar jet sits atop the baroclinicity of the middle latitudes (usually poleward of 30° latitude) and has its speed maxima closer to 300 hPa (e.g. Namias and Clapp 1949, Newton 1954, Palmen and Newton 1969, Keyser and Shapiro 1986, Shapiro and Keyser 1990). The arctic jet is less ubiquitous but is confined to high latitudes and is often located at ~500 hPa (Shapiro et al. 1984, Shapiro 1985, Shapiro et al. 1987).

Careful observational work by Defant and Taba (1957, hereafter DT57) established the existence of a three step structure in tropopause height from pole-to-equator with each step separated from its neighbors by the presence of a westerly wind maximum. The tropical tropopause was found (in the mean) to be at ~90 hPa (17 to 18 km) and to extend to about 30°N. Near that latitude, the tropopause height abruptly lowers to ~200 hPa. The subtropical jet is coincident with this break in tropopause height and is located at ~200 hPa (12 km). Poleward of this feature was what DT57 called the "middle tropopause" located at ~250 hPa. At the break between this middle tropopause and the even lower polar tropopause is the polar jet, located at ~300 hPa. Modest, shallow baroclinicity in the upper troposphere characterizes the subtropical jet whereas the much deeper and more dramatically baroclinic polar front drapes below the polar jet.

A new insight represented by the DT57 analysis was their construction of maps of tropopause height (in hPa). They referred to sharp, isolated, easily identifiable gradients of tropopause height as "breaklines" (see their Fig. 2). These breaklines were found to be coincident with the axes of the respective jet maxima (e.g. the subtropical jet was located at the breakline between the tropical and middle tropopause)[1]. Such depictions made it instantly clear that, though each jet maximum occupied a climatological latitude band, substantial meanders of each were commonplace. Companion maps of tropopause temperature presented by DT57 clearly demonstrated that when the polar and subtropical jets become latitudinally superposed the tropospheric and stratospheric baroclinicity associated with each jet individually were combined into substantially narrower zones of contrast. The resulting superposed jet structure therefore possessed an anomalous fraction of the pole-to-equator baroclinicity (manifest as available potential energy (APE)).

An alternative method for identifying the tropopause breaklines of DT57 lies in the construction of tropopause maps in potential temperature/potential vorticity (θ/PV) space. Such an approach was advocated by Morgan and Nielsen-Gammon (1998) who demonstrated the utility of maps of θ and wind speed on the so-called dynamic tropopause (defined as a surface of constant Ertel PV (Ertel 1942)) for diagnosing weather systems. In this framework, the DT57 breaklines become regions of large PV gradient on isentropes that cut through the subtropical

---

[1] Equation 1 (to be discussed later) demonstrates that local maxima in the geostrophic wind, $\mathbf{V_g}$, are coincident with large horizontal gradients of quasi-geostrophic potential vorticity (QGPV).

and polar jet cores since such isentropes sample both stratospheric and tropospheric air. Though no definitive consensus exists regarding which isentropic surfaces (or layers) best serve to isolate these important jet-related PV gradients, a number of analyses (e.g. Defant and Taba 1957, Palmen and Newton 1969, Shapiro et al. 1987, Morgan and Nielsen-Gammon 1998, Mecikalski and Tripoli 1998, Shapiro et al. 1999, and Randel et al. 2007) point to a fairly narrow range of acceptable values; 310–320K for the polar jet and 335-345K for the subtropical jet. Given that some variation around these values may exist, though likely not to an obfuscating degree, in the present work we shall consider the 315-330K *layer* as the residence of the polar jet and the 340-355K *layer* as the home of the subtropical jet.

Considered from a PV perspective, the subtropical and polar jets are each associated with local positive PV perturbations at the equatorward edge of the tropopause. Most often, the separate jet cores, as well as the separate PV perturbations, are readily identifiable as illustrated in Figs. 1a&b. Note that the PV distribution displayed in Fig. 1b portrays the 3-step tropopause structure identified by DT57. Note also that the separate polar and subtropical jet cores, though widely separated in latitude and elevation, are each found at a "break" in dynamic tropopause height represented by a locally steep tropopause slope. A superposed jet structure cannot be identified solely by inspection of the distribution of isotachs on an isobaric surface (Fig. 1c). Instead, the distinguishing structural characteristic of such jet structures is the vertical tropopause wall directly connecting the tropical tropopause to the polar tropopause (Fig. 1d). The development of such a structure has dynamical implications that are most simply considered from the quasi-geostrophic PV (QGPV) perspective. Recalling that QGPV is given by

$$q_g = \frac{1}{f_o}\nabla^2\phi + f + \frac{f_o^{\,2}}{\sigma}\frac{\partial^2\phi}{\partial p^2} = \Lambda(\phi) + f$$

(where $\Lambda = \frac{1}{f_o}\nabla^2 + \frac{f_o^2}{\sigma}\frac{\partial^2}{\partial p^2}$) then the cross-jet gradient of QGPV is given by

$$\frac{\partial q_g}{\partial n} = \Lambda(\frac{\partial \phi}{\partial n}) = \Lambda(-fV_g) \qquad (1)$$

after substituting from the natural coordinate expression for the geostrophic wind. The deep tropopause wall arises via an increase in $\frac{\partial q_g}{\partial n}$ through a deep layer (i.e. $-\frac{\partial}{\partial p}[\frac{\partial}{\partial t}(\frac{\partial q_g}{\partial n})] > 0$). It follows from (1) that in such an environment

$$f\Lambda[\frac{\partial}{\partial t}(\frac{\partial V_g}{\partial p})] > 0.$$

Since $\Lambda$ is a Laplacian operator, this implies that the development of a deep tropopause wall requires a local increase in the (geostrophic) vertical shear (i.e. $\frac{\partial}{\partial t}(-\frac{\partial V_g}{\partial p}) > 0$). Thus, it is hypothesized that superposition of the polar and subtropical jets can bring about rapid and substantial increases in jet speeds as well as strengthening of the associated divergent ageostrophic circulations.

A number of previously examined high impact, mid-latitude sensible weather phenomena have been connected, either directly or indirectly, with jet superposition events. Defant (1959) noted that an exceptional surface cyclogenesis event south of Iceland on 8 January 1956, in which the sea-level pressure (SLP) dropped 61 hPa in 20 h, developed in an environment characterized by a dramatic jet superposition event. Other famous explosive cyclogenesis events such as the Great October Storm (Hoskins and Berrisford 1988), the ERICA IOP-4 storm (Shapiro and Keyser 1990), the Cleveland Superbomb (Hakim et al. 1996), and the Storm of the

Century (Bosart et al. 1996) are all examples of developments likely influenced by a jet superposition event[2].

More recently, Winters and Martin (2014) examined the influence the secondary circulation associated with a superposed jet structure had in forcing a rapid increase in poleward moisture flux that fueled the second day of the 2010 Nashville Flood. In addition, the 25-28 April 2011 severe weather outbreak across the central and eastern portion of North America (Christenson and Martin 2012 and Knupp et al. 2013) has been linked to a superposed jet structure that formed over the west Pacific Ocean.

Despite the appearance of jet superposition events as a fundamental ingredient in a number of high impact, mid-latitude weather environments, there is no synoptic-climatology of these features nor any systematic study of the mechanism(s) by which the polar and subtropical jets become vertically superposed. It is the goal of this paper to provide a synoptic-climatology.

The paper is organized as follows. Section 2 provides a description of the data sets and methodology used to objectively identify the polar jet, subtropical jet, and locations where the two are vertically superposed. Section 3 presents the results of a 51 year synoptic-climatology of the frequency and distribution of each species of tropopause-level jet. The climatology of jet superposition events is presented in Section 4. Finally, Section 5 discusses the results in the context of other studies of jet stream climatology and offers final comments and conclusions, along with suggestions for future work.

## 2. Data and methodology

[2] At some point in their respective evolutions, all of these cases were characterized by a two-step tropopause structure similar to that portrayed in Fig. 1d.

The climatology is constructed from 51 years of National Center for Environmental Prediction – National Center for Atmospheric Research (NCEP-NCAR) reanalysis data, at 6 hour intervals, spanning the period 1 January 1960 to 31 December 2010. The NCEP-NCAR reanalysis data are available at 17 isobaric levels (1000, 925, 850, 700, 600, 500, 400, 300, 250, 200, 150, 100, 70, 50, 30, 20, and 10 hPa) with a 2.5° latitude-longitude grid spacing (Kalnay et al. 1996, Kistler et al. 2001). These data were bi-linearly interpolated onto isentropic surfaces at 5K intervals from 300K to 370K using programs within the General Meteorology Package (GEMPAK) (desJardins et al. 1991).

In order to identify the polar, subtropical and superposed jet streams an automated, objective identification scheme was developed whose criteria can be described with reference to the features illustrated in Fig. 1. Figure 1a clearly portrays two distinct jets located off the west coast of North America with the polar jet feature near the Oregon, Washington border and the subtropical jet zonally oriented over Mexico. A vertical cross section taken through the polar and subtropical jet cores (Fig. 1b) shows that the polar jet, located at approximately 300 hPa, is largely contained within the 315-330K isentropic layer while the subtropical jet core, located at approximately 200 hPa, occupies the 340-355K layer. Additionally, both the polar and the subtropical jets lie at the low PV edge of the strong horizontal PV gradient that separates the upper troposphere from the lower stratosphere within each respective isentropic layer. The PV isertels are locally quite steep in the vicinity of the jet cores. In fact, considering the 2 PVU contour as the dynamic tropopause, it is clear that the tropopause breaklines of DT57, which portrayed the steep slope of the tropopause near the jet axes, are exactly equivalent to regions of large $|\nabla_{\theta} PV|$ in the 1-3 PVU channel, which represents the boundary between the stratosphere and troposphere. Given these basic structural elements, the identification scheme evaluates characteristics of the PV and wind speed distributions in each grid column. Within the 315-330K (340-350K) layer, whenever the magnitude of the PV gradient within the 1-3 PVU channel exceeds an empirically determined threshold value[3] and the integrated wind speed in the 400-100 hPa layer exceeds 30 m $s^{-1}$, we identify a polar (subtropical) jet in that grid column.

Occasionally, the two jets superpose in the vertical, creating a hybrid of both the subtropical and polar jets, as illustrated in Fig. 1c. A vertical cross-section taken through the jet core, as shown in Fig. 1d, thus illustrates that the criteria for both the polar and subtropical jet are identified in a single vertical grid column, identifying a superposed jet. Notice that, rather than the three-step tropopause structure identified by DT57 and shown in Fig. 1b, a superposed jet is characterized by a two-step tropopause structure with a steep tropopause break from the polar to the tropical tropopause. This nearly vertical PV wall (from ~550 hPa to ~150 hPa in this case) is a leading structural characteristic of these features.

The identification scheme is applied to each 6 h analysis time in the 51 year period to objectively identify grid point locations of the subtropical jet, polar jet and jet superposition events[4]. The identifications are then compiled to reveal the spatial and temporal distribution of all three tropopause-level jet species. In addition, the speed and direction of the wind at 250hPa is recorded for each grid column in which a jet superposition is identified.

---

[3] The threshold value is 0.64 x $10^{-5}$ PVU $m^{-1}$ (0.64 x $10^{-11}$ m K $kg^{-1}$ $s^{-1}$) for both the 315-330K and 340-350K layers. This value was determined by extensive analysis of vertical cross-sections through jets in order to determine the minimum value of $|\nabla_\theta PV|$ required to reliably identify the deep tropopause wall characteristic of superposed jets. For each isentropic layer, the threshold value exceeds the 50th percentile for $|\nabla_\theta PV|$ in grid columns located in the 1-3 PVU channel with integrated wind speed exceeding 30 m $s^{-1}$.

[4] The total number of possible identifications for each grid point in each month of a given year is equal to the number of days in the month x 4. (Example: For a given grid point, each January, with 31 days in the month, would have 124 possible identifications.)

## 3. Analysis of jet distributions

In this section the results of the objective identification of the polar and subtropical jet species are presented as frequency distributions in both seasonal and monthly form. The analysis begins by considering the frequency distributions for the polar jet.

### *a. Polar Jet*

#### *i. Seasonal distribution*

During Northern Hemisphere autumn (SON), the polar jet is found most frequently over the eastern portions of North America and the northern portions of the Atlantic Ocean (Fig. 2a). In the Pacific basin the polar jet is distributed rather uniformly with a localized maxima located south of Alaska. Notably, the polar jet is far less frequent over the eastern hemisphere than over the western hemisphere. During the winter months, (DJF), the polar jet exhibits two prominent frequency maxima (Fig. 2b). The first is a narrow, zonally oriented maximum in the western Pacific. The less zonally-oriented maximum in the Atlantic basin extends from central North America northeastward toward the British Isles. The polar jet frequency minimum over much of Eurasia is even more pronounced in winter than in autumn (Fig. 2b). During spring (MAM), the maximum shifts from the Atlantic to the Pacific where the distribution is remarkably uniform across the entire basin (Fig. 2c). During summer (JJA), the polar jet nearly disappears with only infrequent appearances at high latitudes in the northeast Pacific as well as portions of eastern Canada and the north Atlantic (Fig. 2d).

#### *ii. Monthly distribution*

September is characterized by a hemispheric maxima located across the western Atlantic basin and portions of low latitude Canada (Fig. 3a). Broad, low frequency bands characterize the Pacific basin as well as portions of western and central Europe. An abrupt frequency increase across the hemisphere characterizes October with particularly notable increases in frequency occurring over the Pacific basin (Fig. 3b).

The month of October represents the annual polar jet maxima over the higher latitudes of the Eurasian continent with a band of in excess of 5 times per month covering a large swath. The November frequency distribution (Fig. 3c) is broadly similar to October's with a few subtle differences. First, the October frequency maximum in Eurasia disappears. Second, the nearly uniform frequency distribution across the Pacific basin in October transforms into separate November maxima near Japan and south of Alaska. Finally, the axis of maximum polar jet frequency continues its equatorward march in the Atlantic as the hemisphere cools.

In December narrow latitude bands of maximum frequency exist in the western portions of both ocean basins (Fig. 3d). These bands broaden across the basin from west to east indicating greater variability of the flow in the eastern portions of both basins. Also worthy of note is the fact that the axis of greatest frequency in both basins shifts more dramatically equatorward from November to December than at any other time of year.

January has a similar frequency distribution as December with a continued but less dramatic shift equatorward in both basins (Fig. 3e). Interestingly, the polar jet remains much more common in the Atlantic than in the Pacific basin although the west Pacific basin frequency maxima continues to narrow and extend zonally. By February, the Atlantic (Pacific) frequency maxima has decreased (increased) slightly with the only other notable change being a decrease in polar jet frequency extending from the west coast of North America to the south central Plains of the United States (Fig. 3f).

During the spring, the polar jet undergoes a significant transformation during each month with March exhibiting a shift in the hemispheric frequency maxima from the Atlantic to the Pacific (Fig. 3g). The frequency maxima in the Pacific (Atlantic) basin also increases (decreases) during March. While barely noticeable in Fig. 3g, the polar jet shifts 2.5$^{o}$ north during March in the western Pacific basin beginning its poleward migration north for the summer. By April the polar jet has three local maxima straddling approximately 42.5$^{o}$N in the Pacific with the largest one still residing in the western portion of the basin (Fig. 3h). The Atlantic basin maxima - so robust throughout late autumn and winter - is substantially reduced by April. During May the polar jet continues to retreat to higher latitudes, as the maxima decline dramatically across the hemisphere (Fig. 3i). The rapid poleward retreat and frequency reduction the polar jet undergoes throughout the spring months (Figs. 3g-i) is more dramatic than the autumnal transformation illustrated in Figs. 3a-c. Thus, it appears that the fall and spring transformations of the polar jet are asymmetric.

During the summer months, the polar jet feature reaches an annual minimum as the pole to equator temperature gradient is significantly reduced. The polar jet in June is both poleward shifted and substantially less frequent hemispherically (Fig. 3j). The annual Northern Hemisphere minimum in the polar jet frequency occurs in July when the polar jet is absent everywhere except in the high north Atlantic and off the coast of the Pacific Northwest (Fig. 3k). August has only slightly higher polar jet frequency at high latitudes of the Northern Hemisphere (Fig. 3l) suggesting a near absence of the polar jet hemispherically at the height of Northern Hemisphere summer.

*b. Subtropical Jet*

*i. Seasonal distribution*

During autumn, the subtropical jet is found most frequently over the western Pacific basin with a broad, low frequency band that spirals poleward starting over north Africa, extending across both hemispheres, before ending in the eastern Atlantic basin (Fig. 4a). During winter, the subtropical jet reaches its annual frequency maximum across the hemisphere – a characteristic it shares with the polar jet. However, compared to the wintertime polar jet frequency distribution, the subtropical jet is more latitudinally restricted indicating that it is less variable than the polar jet during the winter months[5]. As in autumn, the wintertime subtropical jet frequency maxima spirals poleward from the central Atlantic, across north Africa, southern Eurasia, reaching its hemispheric maxima in the western Pacific, ending poleward of where the distribution band begins in the central Atlantic (Fig. 4b). During spring, the distribution has wider latitudinal extent, but does not spiral poleward. Instead, the frequency maxima rather continuously straddles the same latitude (~ 30°N) across the hemisphere (Fig. 4c). The springtime hemispheric maxima again occurs in the western Pacific, as it does in all seasons. The latitudinal distribution of the subtropical jet is even wider in summer and is displaced substantially poleward as compared to the other seasons (Fig. 4d). The subtropical jet is much more common than the polar jet during the summer months suggesting that the most common jet species involved in Northern Hemisphere mid-latitude summertime weather is the subtropical jet not the polar jet.

*ii. Monthly distribution*

During the month of September, the subtropical jet is found in a wide latitude band in the western Pacific basin with a frequency maxima over the northern Sea of Japan (Fig. 5a). The wide band of low frequency distribution over North America and the north Atlantic testifies to

[5] Figure 4 also makes clear that the subtropical jet is less variable during winter at any other time of year.

the variability of the subtropical jet pattern in these regions during September. The distribution in October looks nearly identical though the Pacific maxima shifts slightly eastward and equatorward (Fig. 5). By November the subtropical jet frequency maxima in the Pacific has consolidated into a narrow latitudinal strip centered on Japan (Fig. 5c). Figures 5a-c demonstrate that, during autumn, the subtropical jet shifts equatorward and becomes narrowly focused over the west Pacific near ~33$^{o}$N.

By December, the axis of maximum subtropical jet frequency has expanded both eastward and westward but remains fixed near 32.5$^{o}$N while the maximum in frequency has increased to greater than 25 times per month in some locations (Fig. 5d). January represents the month of maximum subtropical jet frequency with a large swath of greater than 31 identifications per month along the north coast of Japan (Fig. 5e). January is also the first month that exhibits a thin band of greater than 7 identifications per month stretching westward from the southern portion of Asia to North Africa. February has nearly the same hemispheric distribution as January but with a small reduction in the west Pacific frequency maxima (Fig. 5f). Throughout the winter months, the subtropical jet frequency maxima shifts westward (Figs. 5d-f). The fact that the seasonal average frequency distribution (Fig. 4b) looks very much like that of the individual winter months (Fig. 5d-f) indicates that the subtropical jet is strongly constrained during winter.

Spring is a transition period for the subtropical jet distribution, as it was for the polar jet. The distribution in March is quite similar to the distributions in the preceding winter months albeit with reduced frequencies (Fig. 5g). The distribution in April is a bit of an outlier as the west Pacific frequency maxima nearly disappears amid a notable decrease in frequency globally (Fig. 5h).  By May, on the other hand, the west Pacific frequency maxima is reinvigorated while shifted to slightly higher latitudes (Fig. 5i). The latitudinal band of maximum frequency is also wider as compared to March and the winter months suggesting enhanced variability in the west Pacific subtropical jet during late spring.

June exhibits a maximum in the western Pacific basin and a distribution, from North Africa to the north Atlantic, that spirals toward the pole (Fig. 5j). Compared to May (Fig. 5i) the hemispheric distribution in June is clearly displaced poleward – a trend that continues through the summer months. By July, the western Pacific maximum is no longer evident, but is replaced by an elongated and moderate frequency maxima that stretches westward from the dateline to the central portion of Eurasia. A local maxima is also present in the western Atlantic near the northeast coast of North America (Fig. 5k). The subtropical jet distribution in August is characterized by a broad band of lower frequency across the hemisphere, with isolated small maxima found across Eurasia, the western Pacific, and eastern North America (Fig. 5l).

## 4. Distribution of jet superpositions

As described previously, a jet superposition (alternatively, a *superposed jet*) occurs when both the polar jet and subtropical jet are identified in the same vertical grid column. In this section the frequency distribution of such structures is presented.

*a. Seasonal distribution*

During the autumn, jet superposition events exhibit a broad distribution with relatively low frequency across both the Atlantic and Pacific Ocean basins (Fig. 6a)[6]. Winter is dramatically different than autumn, as a hemispheric maximum in jet superposition occurs in the

[6] Note that the number of identifications each month is on the order of 2-4% of those of the individual jet species, testifying to the relative rarity of jet superposition.

western Pacific basin; straddling the latitudes of maximum frequency of the polar and subtropical jets (Fig. 6b). Local maxima of low frequency are also present over southern North America with a more limited maxima over North Africa. By spring a drastic decline in the number of superposition events is evident across the hemisphere, especially in the western Pacific basin (Fig. 6c). During the summer months, superposition events become exceptionally infrequent with the annual minimum occurring during the month of July (not shown) coincident with the near disappearance of the polar jet in summer months.

*b. Monthly distribution*

September superposition events are most common in the western Pacific basin and in the north Atlantic (Fig. 7a). The two ocean basins are characterized by frequency maxima as a result of the proximity of the polar jet (Fig. 3a) to the subtropical jet (Fig. 5a) in these locations. By October, both frequency maxima have expanded in areal extent – the Pacific maxima to the east and the Atlantic maxima to the southwest (Fig. 7b). In November the Pacific distribution narrows latitudinally while the north Atlantic frequency maxima has retracted to the southwest, west of the British Isles (Fig. 7c).

By December, the local maximum in jet superposition events in the western Pacific first presents itself (Fig. 7d). This dramatic increase results from an increased frequency, as well as a decreased variability, of both the subtropical and polar jets in this region at this time of year. In fact, in December the axis of maximum frequency of the two jet species are typically separated by only a few degrees of latitude in the west Pacific. The west Pacific frequency maxima reaches its annual peak just east of Japan in January (Fig. 7e).This increased frequency appears related to an increased frequency of the subtropical jet. Despite a coherent increase in the polar jet frequency, the frequency of jet superpositions in the west Pacific decreases in February (Fig. 7f).

In fact, despite the frequency and close proximity of the polar and subtropical jets during west Pacific winter, evident through a comparison of Figs 3d-f and Figs. 5d-f, vertical superposition of the two species remains a rare event.

Despite the annual maximum in Pacific basin polar jet frequency that characterizes March (Fig. 3g), the number of jet superpositions significantly decreases there in the same month (Fig. 7g). This decrease in frequency is likely tied to the corresponding decrease in the subtropical jet frequency (Fig. 5g). In April, a nearly complete absence of jet superpositions is observed throughout the hemisphere (Fig. 7h), seemingly related to the poleward march of the increasingly variable polar jet (Fig. 3h), coupled with a rapid decrease in the frequency of the subtropical jet, especially in the west Pacific (Fig. 5h). During May, the frequency of west Pacific jet superpositions recovers in areal extent but is characterized by low frequency in the basin (Fig. 7i). Though not shown, jet superpositions continue to decrease in frequency, with a seasonal minimum occurring during the month of July, corresponding to the summer minimum of the polar jet (Fig. 3k).

*c. Additional characteristics of superposed jets*

In order to further characterize the nature of superposed jets, for each event identified in the 51 year climatology we examined the wind direction and speed at 250 hPa for the months of September-April. The average 250 hPa wind speed associated with all superpositions observed during September is 68.5 m $s^{-1}$ while the most common wind direction associated with September superpostions is southwesterly, with SSW, WSW, and W accounting for a significant portion of the total number of September superpositions (Fig. 8a). The average wind speed increases to 71.9 m $s^{-1}$ during October as WSW becomes the predominant direction with W and SW also well represented in the distribution (Fig. 8b). By November, the primary wind direction characterizing jet superpositions becomes more solidly WSW while the average wind speed increases to 77.0 m $s^{-1}$ (Fig. 8c). December has nearly as many WSW as W jet superpositions which are accompanied by an increase in the average wind speed to 83.5 m $s^{-1}$ (Fig. 8d). The primary wind direction for January jet superpositions veers back to westerly as over half of the superpositions in January are associated with a west wind (Fig. 8e). The average wind speed also continues to increase reaching 90.1 m $s^{-1}$ by this time. These observations make clear that superposed jets are some of the strongest jets found in the hemisphere. The speed and direction characteristics of February are nearly identical to January's with over half of superpositions associated with a westerly wind, while the average wind speed increases fractionally to 90.3 m $s^{-1}$ (Fig. 8f). As spring arrives in the Northern Hemisphere the average wind speed of jet superpositions decreases to 83.0 m $s^{-1}$ in March (Fig. 8g). The wind direction also begins to back as WSW is, once again, established as the most frequent wind direction. By April, the average wind speed decreases to 66.2 m $s^{-1}$, a nearly 24 m $s^{-1}$ decrease in just two months (Fig. 8h). These data illustrate an asymmetry in the annual evolution of superposed jets as the vernal decrease in average wind speed is considerably more rapid than the autumnal increase.

*d. Comparison to DJF mean zonal wind*

The Northern Hemisphere tropopause-level flow is often considered from the perspective of the zonal mean wind at some upper tropospheric isobaric level. Though this perspective is analytically simple, it fails to account for the more complicated distribution of the polar and subtropical jets revealed by the preceding analysis. Figure 9 illustrates aspects of the obfuscation engendered by this popular approach. The wintertime polar jet frequency maxima lie on the poleward edge of the 250 hPa seasonal mean zonal wind around the entire Hemisphere (Fig. 9a). In addition, the portions of the eastern Pacific and North Atlantic where the 250 hPa zonal mean wind fails to reach 30 m $s^{-1}$ and yet the polar jet is found with regularity, suggests that the polar jet is highly variable in those regions. The subtropical jet frequency maxima, on the other hand, are found in the core of the average zonal wind isotachs from North Africa eastward to the central Pacific (Fig. 9b) suggesting a prominent role for the subtropical jet in the annual tropopause-level wind climatology over this vast area. Over North America, however, the subtropical jet is found on the equatorward edge of the average 250 hPa zonal wind, suggesting that the average zonal wind in this region is nearly equally composed of polar jet and subtropical jet components. The jet superposition frequency maximum in the Pacific is displaced eastward and slightly poleward of the zonal wind maximum there. Whether this distribution suggests that superposition events in the west Pacific preferentially result from equatorward excursions of the polar jet at the entrance to the Pacific storm track is a subject for future inquiry. Similarly intriguing is the fact that the superposition maximum in the Atlantic is nearly coincident with the local zonal wind maximum (Fig. 9c).

## 5 - Summary and Discussion

Jet streams or jets, defined as narrow, rapidly flowing currents of air located near the tropopause, often play a significant role in sensible weather in the mid-latitudes. Two species of jets have been identified in prior studies, the polar jet and the subtropical jet. The dynamics and characteristics of these two separate jet species were first considered in several studies undertaken in the 1940s and 50s. Namias and Clapp (1949) first discussed the tropospheric jet stream from the perspective of confluence, which drives horizontal frontogenesis. In addition, they made observations about the presence of the polar front, tropopause breaks, and suggested that the jets were weaker and further poleward during summer than winter. Yeh (1950), Koteswaram (1954), and Krishnamurti (1961) examined the tropospheric circulations over India and China, particularly during the winter months, and made the first discoveries of the west Pacific subtropical jet.

Some of the most significant findings regarding the large scale distribution of Northern Hemisphere jet streams were advanced by DT57, when they first published horizontal maps of tropopause heights. Since its introduction in 1957, the only amendment to DT57's conception of a three step tropopause structure came from Shapiro (1987), who suggested the addition of the arctic jet and arctic tropopause step. Riehl (1962) appears to have been the first to suggest that the polar and subtropical jets were found within close proximity to each other in the west Pacific (Riehl 1962 Fig. 1.2), a suggestion supported by the analysis presented in this paper.

In their examination of the distribution of Northern Hemisphere jet streams, Koch et al. (2006) used an integrated wind speed threshold to identify the jet streams. They further subdivided their jet identification into two subcategories; those jet features with shallow baroclinicity were classified as subtropical jets while those with deep baroclinicity were classified as polar jets. Broadly speaking, the results of their shallow baroclinicity classification correlate well with the findings presented in our work (their Fig. 6 compared to our Fig. 4). When the deep baroclinicity classification is compared however, significant differences exist (their Fig. 7 and our Fig. 2). First, their winter maximum in the deep baroclinicity (polar) jet in the Atlantic is less expansive that the Atlantic polar jet frequency maximum reported in the present analysis. Second, the Pacific basin is significantly different, with two maxima present in the Koch et al. analysis while, a single latitude band maxima is present in our analysis (Fig. 2b). Finally, our analysis for spring indicates a local maxima in the western Pacific basin (Fig. 2c), while Koch et al. show a polar jet maximum in the central Pacific. Summer and autumn are broadly consistent between the two climatologies.

Unfortunately, the Koch et al. (2006) classification scheme is not amenable to the identification of jet superposition events. The identification scheme introduced in this paper, which takes into account an integrated wind speed as well as a PV gradient threshold within specified isentropic layers, allows each jet type to be identified separately and so also allows identification of jet superpositions.

With respect to jet superpositions, only in the western Pacific basin during winter do they occur with regularity (Fig. 6b). Interestingly, despite the proximity of the polar jet (Fig. 2b) and the subtropical jet (Fig. 4b) in the Pacific, jet superpositions are still relatively rare. The analysis presented here finds that jet superpositions exhibit a broad, low frequency distribution over both ocean basins during autumn (Fig. 6a), and that they are nearly absent during the Northern Hemisphere summer, coincident with the absence of the polar jet over most of the hemisphere.

The average wind speed at 250 hPa associated with jet superpositions steadily increases during fall to a wintertime maximum of 90.3 m $s^{-1}$ during February. The average wind speed associated with these features decreases more rapidly during spring than it increases during fall, illustrating an asymmetric distribution of wind speed tendency associated with the annual cycle of jet superpositions. A possible explanation for this asymmetry is the unique presence of tropical cyclones in the autumn. Tropical cyclones (TCs) are associated with a positive tropopause $\theta$ anomaly directly above the storm itself as well as in its vast outflow area. TCs can migrate to the mid-latitudes while maintaining such large-scale thermal signatures. Since the subtropical jet is tied to the region of large subtropical tropopause slope (i.e. large $\nabla\theta$ on the subtropical dynamic tropopause), the poleward recurving of TCs offers a number of opportunities for jet superposition that are unavailable in the TC-free spring.

The analysis and methodology presented in this paper provide a framework for objective identification of the tropopause-level polar and subtropical jets. Without a means to separately identify these two species, studies of the polar jet, sometimes difficult to distinguish from the subtropical westerlies (Barnes and Polvani, 2013) have been done by proxy. Recent emphasis on the "eddy-driven jet" (Hartmann 2007, Woollings et al. 2010, Barnes and Polvani 2013), defined in the lower troposphere (below the 700 hPa level), is one example. Despite the physical insights garnered by such studies, it is clear that use of the eddy-driven jet as a proxy for describing the polar jet inadequately accounts for the polar jet structure or its important dynamics. For instance, the eddy-driven jet perspective precludes consideration of the tropopause break identified by DT57 as a characteristic of the polar jet. Additionally, geostrophic cold air advection along the polar jet often results in downward extrusion of stratospheric PV into the upper troposphere above 700 hPa (Shapiro 1981, Keyser and Pecnick 1985, Martin 2014), leading to the production of mid-tropospheric features that are ultimately responsible for the development of surface cyclones. Such important structural and dynamical characteristics of polar jet life cycles are inscrutable from the alternative eddy-driven jet perspective.

Previous work has found that, directly or indirectly, jet superposition structures are associated with high impact weather events. The first such example, described by Defant (1959), involved a jet superposition that was a component of a large scale environment associated with a north Atlantic surface cyclogenesis event in which the SLP minimum deepened 61 hPa in 20 h. Other work has focused on PV streamers and their presence in association with extreme precipitation events over western Europe (Massacand et al. 1998, 2001, Martius et al 2006, etc). In addition, floods in northwest Africa (Knippertz and Martin 2005, 2007a,b), atmospheric rivers

(Zhu and Newell 1998), and other explosive cyclogenesis events such as the Cleveland Superbomb (Hoskins and Berrisford 1988) all seem to be associated with jet superpositions.

More recently, Winters and Martin (2014) investigated the role that a jet superposition played in the May 2010 Nashville flood event. They found that the poleward moisture flux accomplished by the secondary ageostrophic circulation associated with the upper troposphere jet structure increased 120% following superposition of the polar and subtropical jets. This increased moisture flux acted to further enhance the precipitation on the second day of the event, leading to catastrophic flooding in Nashville and other portions of Tennessee. The 25-28 April 2011 severe weather outbreak in central North America is another example from a growing list of high impact weather events associated with jet superpositions (Christenson and Martin 2012 and Knupp et al. 2013).

The work presented in this study motivates a number of additional research questions. One such question regards the frequency distributions of the polar, subtropical, and jet superpositions in the Southern Hemisphere. Additionally, given that in the western Pacific the polar and subtropical jets are frequently in very close proximity to one another during the winter (as first suggested by Riehl (1962)), why is vertical superposition still so rare? As suggested by Winters and Martin (2014), consideration of the polar and subtropical jets as related to separate PV perturbations on the tropopause affords some insights into this problem (Fig. 10). Each PV perturbation has a cyclonic circulation associated with it that extends above and below the level of the anomaly. In the space between the two anomalies there is destructive interference between the circulations associated with the two PV anomalies. This interference results in a wind speed minima in that overlapping region that may act as a natural barrier to superposition. Winters and Martin (2013) hypothesize that a combination of convective heating equatorward of the subtropical jet and internal jet dynamics (e.g. geostrophic shearing deformation) may work in concert to eliminate this barrier to jet superpositions. The convective heating can erode the PV equatorward of the subtropical jet serving to either steepen the tropopause locally (as was the case in the west Pacific in April 2011) or displace the tropical/subtropical tropopause break poleward as appears to have been the case during the evolution of the superposed jet that characterized the Nashville Flood case (Winters and Martin 2013). Internal jet dynamics may be manifest as geostrophic warm air advection in cyclonic shear along the subtropical jet (Lang and Martin 2013) which is associated with ascent through the subtropical jet core and subsidence to its poleward side as illustrated in Fig. 10.

Additional future work, with implications for understanding changes in the general circulation in a warmer climate, will apply our identification scheme to the output from selected CMIP5 simulations. As the evidence for Arctic amplification increases and the pole-to-equatorward temperature gradient relaxes in the lower troposphere, it is plausible that a warmer planet will be characterized by a hemispheric reduction of the polar jet. However, given the moist neutrality of the tropical atmosphere, any warming of the surface will be reflected by larger warming aloft. Therefore it is not inconceivable that a warmer planet will feature enhanced baroclinicity in the tropical/subtropical upper troposphere – lower stratosphere (UTLS), thus supporting a stronger subtropical jet.

Finally, the interaction between, and superposition of, the polar and subtropical jets – which has served as the focus of this paper – represents perhaps one of the most conspicuous and synoptic-scale manifestations of tropical/extratropical interaction. To the extent that the frequency and distribution of these features, along with the synoptic and mesoscale dynamics associated with them, are better understood, so will be the diagnoses and prognoses of weather systems in both the current and future climate.

# REFERENCES


Barnes, Elizabeth A., Lorenzo Polvani, 2013: Response of the Midlatitude Jets, and of Their Variability, to Increased Greenhouse Gases in the CMIP5 Models. *J. Climate*, **26**, 7117–7135.

Bosart, L. F., G. J. Hakim, K. R. Tyle, M. A. Bedrick, W. E. Bracken, M. J. Dickinson, and D. M. Schultz, 1996: Large-scale antecedent conditions associated with the 12-14 March 1993 cyclone (“Superstorm ’93”) over eastern North America. *Mon. Wea. Rev.*, **124**, 1865-1891.

Christenson, C. E., and J. E. Martin, (2012, March). The Large-scale environment associated with the 25-28 April 2011 severe weather outbreak. Presented at the Meeting of National Weather Association, Des Moines, Ia.

Defant, F., 1959: On hydrodynamic instability caused by an approach of subtropical and polarfront jet stream in northern latitudes before the onset of strong cyclogenesis. *The Atmosphere and Sea in Motion*, Ed. Bert Bolin, Rockefeller Institute Press, New York, NY., 305-325.

_____, and H. Taba, 1957: The threefold structure of the atmosphere and the characteristics of the tropopause. *Tellus*, **9**, 259-275.

desJardins, M. L., K. F. Brill, and S. S. Schotz, 1991: Use of GEMPAK on UNIX workstations. *$7^{th}$ Int, conf. on Interactive Information and Processing Systems for Meteorology, Oceanography, and Hydrology*, New Orleans, LA, Amer. Meteor. Soc., 449-453.

Ertel, 1942b: Ein neuer hydrodynamischer Wirbelsatz. *Meteor. Z.,* **59,** 277–281.

Hakim, G. J., D. Keyser, and L. F. Bosart, 1996: The Ohio Valley wave merger cyclogenesis event of 25-26 January 1978. Part II: Diagnosis using quasigeostrophic potential vorticity inversion. *Mon. Wea. Rev.*, **124**, 2176-2205.

Hartmann, D.L., 2007: The General Circulation of the Atmosphere and its Variability. *J. Meteor. Soc. Japan***, 85B**, 123-143.

Hoskins, B. J., and P. Berrisford, 1988: A potential vorticity perspective of the storm of 15-16 October 1987. *Weather*, **43**, 122-129.

Kalnay et al.,The NCEP/NCAR 40-year reanalysis project, Bull. Amer. Meteor. Soc., 77, 437-470, 1996.

Kistler, Robert, and Coauthors, 2001: The NCEP–NCAR 50–Year Reanalysis: Monthly Means CD–ROM and Documentation. *Bull. Amer. Meteor. Soc.*, **82**, 247–267.

Keyser, Daniel, Michael J. Pecnick, 1985: A Two-Dimensional Primitive Equation Model of Frontogenesis Forced by Confluence and Horizontal Shear. *J. Atmos. Sci.*, **42**, 1259–1282.

______, D. and M. A. Shapiro, 1986: A review of the structure and dynamics of upper-level frontal zones. *Mon. Wea. Rev.*, 114, 452-499.

Knippertz, P., and J. E . Martin, 2005: Tropical plumes and extreme precipitation in subtropical and tropical West Afric., *Quart. J. Roy. Meteor. Soc.*, **131**, 2337-2365.

____ and ____, 2007a: The role of large-scale dynamic and diabatic processe s in the generation of cut-off lows over Northwest Africa. *Meteorol. Atmos. Phys.*,**96**,3 19.

_____, and _____, 2007b: A Pacific moisture conveyor belt and its relationship to an unusual precipitation event in the semi-arid southwestern United States. *Wea. Forecasting*,**22**, 125-144.

Knupp, Kevin R. et al., 2013: Meteorological Overview of the Devastating 27 April 2011 Tornado Outbreak. *Bull. Amer. Meteor. Soc., Early Online Release.*

Koch, P., H. Wernli, and H. C. Davies, 2006: An event-based jet-stream climatology and typology. *Int. J. Climatol*., **26**, 283-301.

Koteswaram, P. 1953: An analysis of the high tropospheric wind circulation over India in winter. *Indian J. Meteor. Geophys*., **4**, 13-21.

_____, and S. Parthasarathy, 1954: The mean jet stream over India in the pre-monsoon and post-monsoon seasons and vertical motions associated with subtropical jet streams. *Indian J. Meteor. Geophys*., **5**, 138-156.

Krishnamurti, T. N., 1961: The subtropical jet stream of winter. *J. Meteor*., **18**, 172-191.

Lang, A. A., and J. E. Martin, 2014: The structure and evolution of lower stratospheric frontal zones. Part II: The influence of tropospheric convection on lower stratospheric frontal development. *Quart. J. Roy. Meteor. Soc.*, **138**, (in press).

Loewe, F., and V. Radok, 1950: A meridional aerological cross section in the Southwest Pacific. *J. Meteor*., **7**, 58-65. (Revised 305-306).

Martin, J. E., 2014: Quasi-gesotrophic diagnosis of the influence of vorticity advection on the development of upper level jet-front systems. *Quart. J. Roy. Meteor. Soc.*,**140** (in press).

Martius, O., E. Zenklusen, C. Schwierz, and H. C. Davies, 2006: Episodes of alpine heavy precipitation with an overlying elongated stratospheric intrusion: A climatology. *Int. J. Climatol*., **26**, 1149-1164.

Massacand, A. C., Wernli, H., and H. C. Davies, 1998: Heavy precipitation on the Alpine southside: An upper-level precursor. *Geophys. Res. Let*., **25**, 1435-1438.

_____, _____, and _____, 2001: Influence of upstream diabatic heating upon an Alpine event of heavy precipitation. *Mon. Wea. Rev*., **129**, 2822-2828.

Mecikalski, J. R., and G. J. Tripoli, 1998: Inertial available kinetic energy and the dynamics of tropical plume formation. *Mon. Wea. Rev*., **126**, 2200-2216.

Mohri, K., 1953: On the fields of wind and temperature over Japan and adjacent waters during winter of 1950-1951. *Tellus,* **5**, 340-358.

Morgan, M. C., and J. W. Nielsen-Gammon, 1998: Using tropopause maps to diagnose midlatitude weather systems. *Mon. Wea. Rev*., **126**, 2555-2579.

Namias, Jerome, Philip F. Clapp, 1949: Confluence theory of the high tropospheric jet stream. *J. Meteor.*, **6**, 330–336.

Newton, C. W., 1954: Frontogenesis and frontolysis as a three-dimensional process. *J. Meteor.*, **11**, 449-461.

Palmén, E., and C. W. Newton, 1969: *Atmospheric Circulation Systems: Their Structure and Physical Interpretation*. Academic Press, 603 pp.

Randel, W. J., D. J. Seidel, and L. L. Pan, 2007: Observational characteristics of double tropopauses. *J. Geophys. Res*., **112**, D07309, doi:10.1029/2006JD007904.

Riehl, H., 1962: Jet streams of the atmosphere, *Technical Report No. 32*. Department of Atmospheric Science, Colorado State University, Fort Collins, CO, 117.

Shapiro, M. A., 1981: Frontogenesis and geostrophically forced secondary circulations in the vicinity of jet stream-frontal zone systems. *J. Atmos. Sci*., **38**, 954-973.

_____, 1985: Dropwindsonde observations of an Icelandic Low and a Greenland mountain-lee wave. *Mon. Wea. Rev*., **113**, 680-683.

_____, M. A., Oltmans, S.J., Bodhaine, B.A. and Schnell, R.C. (1984). El Chichon volcanic debris in an Artic tropopause fold. Geophysical Research Letters 11: doi:10.1029/0GPRLA000011000005000421000001.

_____, T. Hampel, and A. J. Krueger, 1987: The Arctic tropopause fold. *Mon. Wea.Rev*., **115**, 444-454.

_____, and D. Keyser, 1990: Fronts, jet streams and the tropopause. *Extratropical Cyclones: The Erik Palmen Memorial Volume*, C. Newton and E. O. Holopainen, Eds., Amer. Meteor. Soc., 167-191.

_____, H. Wernli, J. Bao, J. Methven. X. Zou. J. Doyle, T. Holt, E. Donall-Grell, and P. Neiman, 1999: A planetary-scale to mesoscale perspective of the life cycles of extratropical cyclones: The bridge between theory and observations. *The Life Cycle of Extratropical Cyclones*, Eds. M. A. Shapiro and S. Gronas, Amer. Meteor. Soc., 139-185.

Sutcliffe, R. C., and J. K. Bannon, 1954: *Seasonal changes in the upper-air conditions in the Mediterranean Middle East area*. Sci. Proc. International Assoc. Meteor. (UGGI), Rome 1954.

Winters, A.C., and J. E. Martin. (2013, October). Investigation of the dynamical mechanisms facilitating jet superposition during the 2010 Nashville flood. Presented at the Meeting of 16th Cyclone Workshop, Sainte Adele, Quebec, Canada.

_______, A. C., and J. E. Martin, 2014: The role of a polar/subtropical jet superposition in the May 2010 Nashville Flood. *Wea. Forecasting*,**29**, (submitted)

Woollings, T., A. Hannachi and B. Hoskins, 2010: Variability of the North Atlantic eddy-driven jet stream, Q. J. R. Meteorol. Soc., 649, 856-868.

Yeh, T. C., 1950: The circulation of the high troposphere over China in the winter of 1945-46. *Tellus*, **2**, 173-183.

Zhu, Y., and R. E. Newell, 1998: A proposed algorithm for moisture fluxes from atmospheric rivers. *Mon. Wea. Rev.*, **126**, 725-735.

# LIST OF FIGURES

**Figure 6:** (a) Average frequency of Northern Hemisphere jet superpositions during the three month period September-November over the period 1960-2010. (b) As in Fig. 6a but for the months of December-February. (c) As in Fig. 6a but for the months of March-May.

**Figure 7:** (a) Average frequency of Northern Hemisphere jet superpositions during the month of September over the period 1960-2010. (b) As in Fig. 7a but for October. (c) As in Fig. 7a but for November. (d) As in Fig. 7a but for December. (e) As in Fig. 7a but for January. (f) As in Fig. 7a but for February.

**Figure 7 (continued):** (g) As in Fig. 7a but for March. (h) As in Fig. 7a but for April. (i) As in Fig. 7a but for May.

**Figure 8:** (a) Wind direction plotted on the wind rose for every Northern Hemisphere jet superposition identified during the month of September over the period 1960-2010. Average wind speed for each jet superposition in $m\ s^{-1}$ shown in blue on bar graph. (b) As in Fig. 8a but for but for October. (c) As in Fig. 8a but for but for November. (d) As in Fig. 8a but for but for December.

**Figure 8 (continued):** (e) As in Fig. 8a but for but for January. (f) As in Fig. 8a but for but for February. (g) As in Fig. 8a but for but for March. (h) As in Fig. 8a but for but for April.

**Figure 9:** (a) DJF seasonal average frequency of polar jet identification (fill) and isotachs of average zonal (U-wind) at 250hPa (black contour) every 10 $m\ s^{-1}$ starting at 30 $m\ s^{-1}$ over the period 1960-2010. (b) As in Fig. 9a but with fill indicating subtropical jet identifications. (c) As in Fig. 9a but with fill indicating jet superposition identifications.

**Figure 10:** Schematic vertical cross section illustrating the dynamical processes that may Facilitate a superposition of the polar (PJ) and subtropical (STJ) jet. Each jet is associated with a tropopause level positive PV perturbation (signified by the + signs). Corresponding circulations at and below each perturbation are indicated by a circled x or ●. Solid black line is the 1.5 PVU isosurface with the lower stratosphere shaded gray. See text for explanation. (Adapted from Winters and Martin 2014).

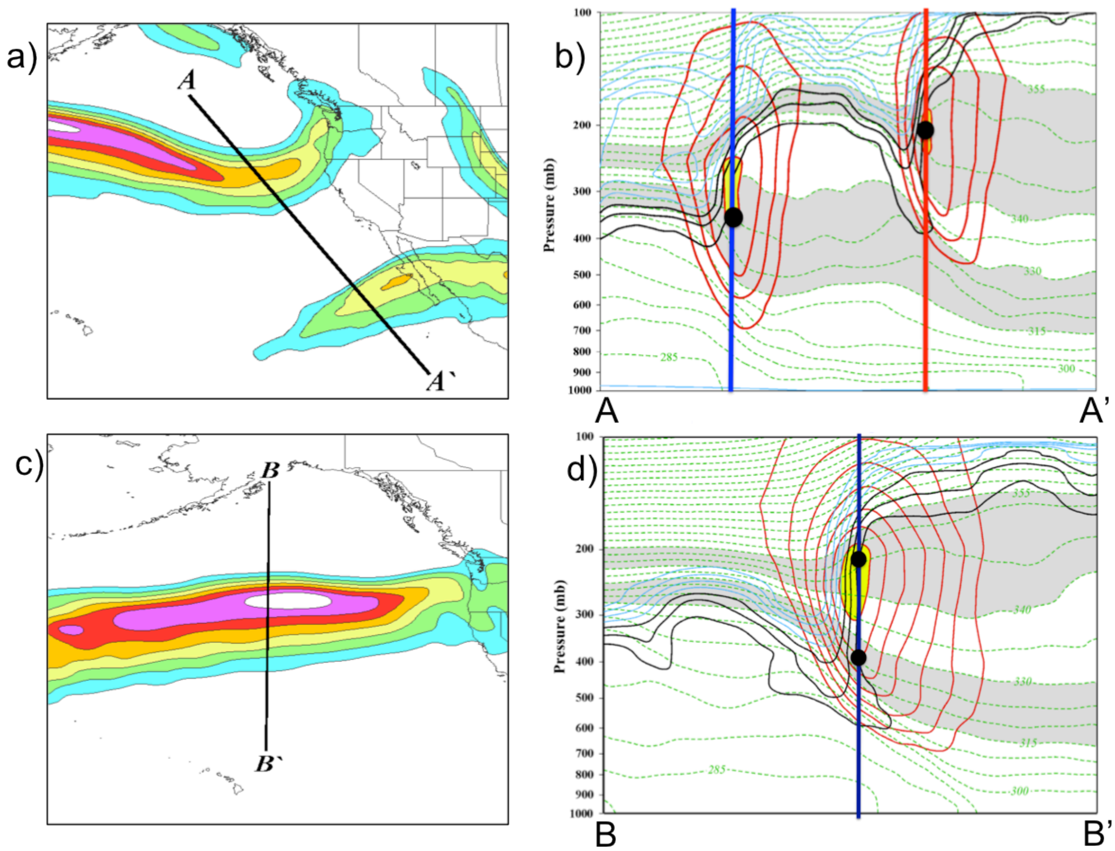


**Figure 1:** (a) 300 hPa isotachs (shaded every 10 m s $^{-1}$ starting at 30 m s$^{-1}$) at 0000 UTC 27 April 2010 depicting separate polar and subtropical jets. (b) Cross section along A-A' in Fig. 1a. Solid black (blue) lines are isertels of 1, 2, 3 (4-9) PVU (1 PVU = $10^{-6}$ K m$^{2}$ kg$^{-1}$ s$^{-1}$). Dashed lines are isentropes contoured every 5K. Red solid lines are isotachs labeled in m s-1 and contoured every 10 m s-1 starting at 30 m s-1. The jet cores are shaded yellow and the 315-330K and 340-355K isentropic layers, used to identify the location of the jets, are shaded gray. The blue (red) line corresponds to a grid column in which the black dot confirms a polar (subtropical) jet identification. (c) As in (a) but at 0000 UTC 24 October 2010. (d) As in (b) but along the cross section B-B' in Fig. 1c, The blue line corresponds to a grid column in which a jet superposition (i.e. a polar and subtropical jet in the same column) is identified.

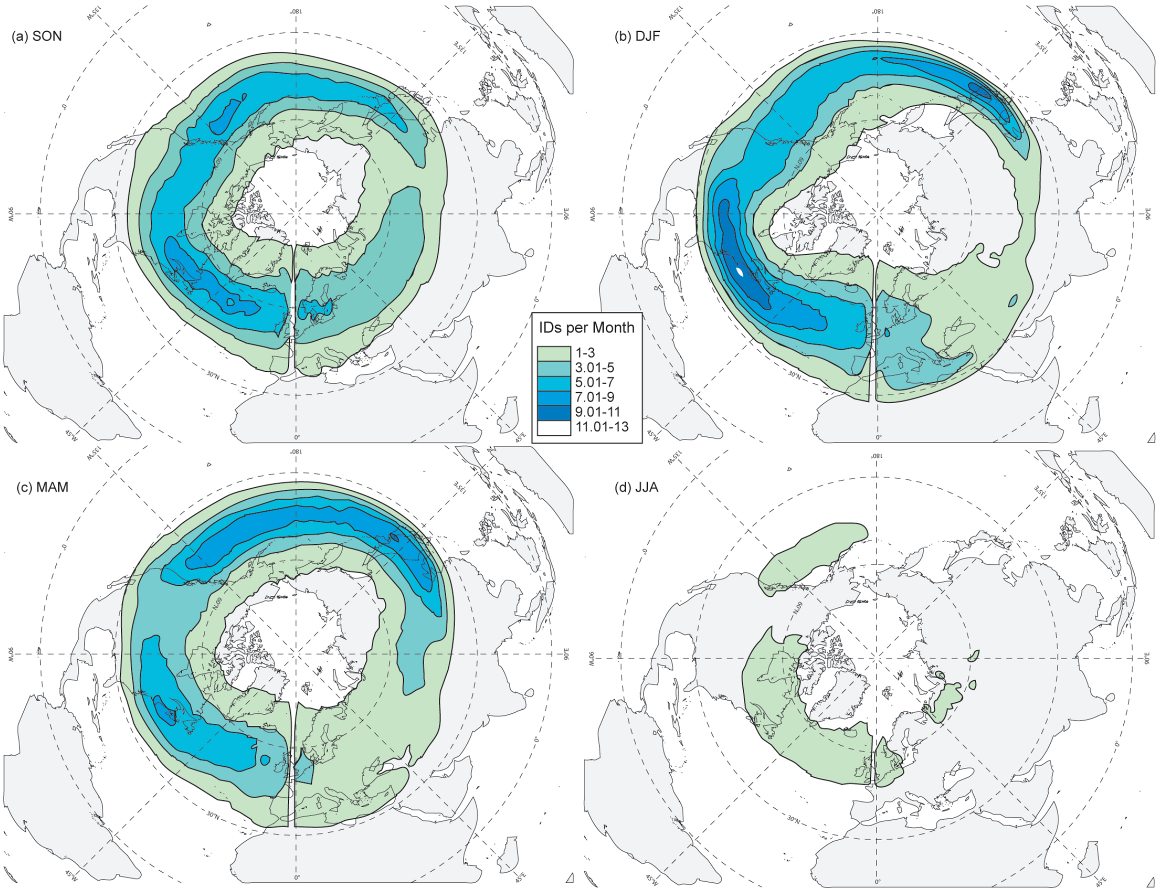


**Figure 2:** (a) Average frequency of Northern Hemisphere polar jet identifications during the three month period September-November over the period 1960-2010. (b) As in Fig. 2a but for the months of December-February. (c) As in Fig. 2a but for the months of March-May. (d) As in Fig. 2a but for the months of June-August.

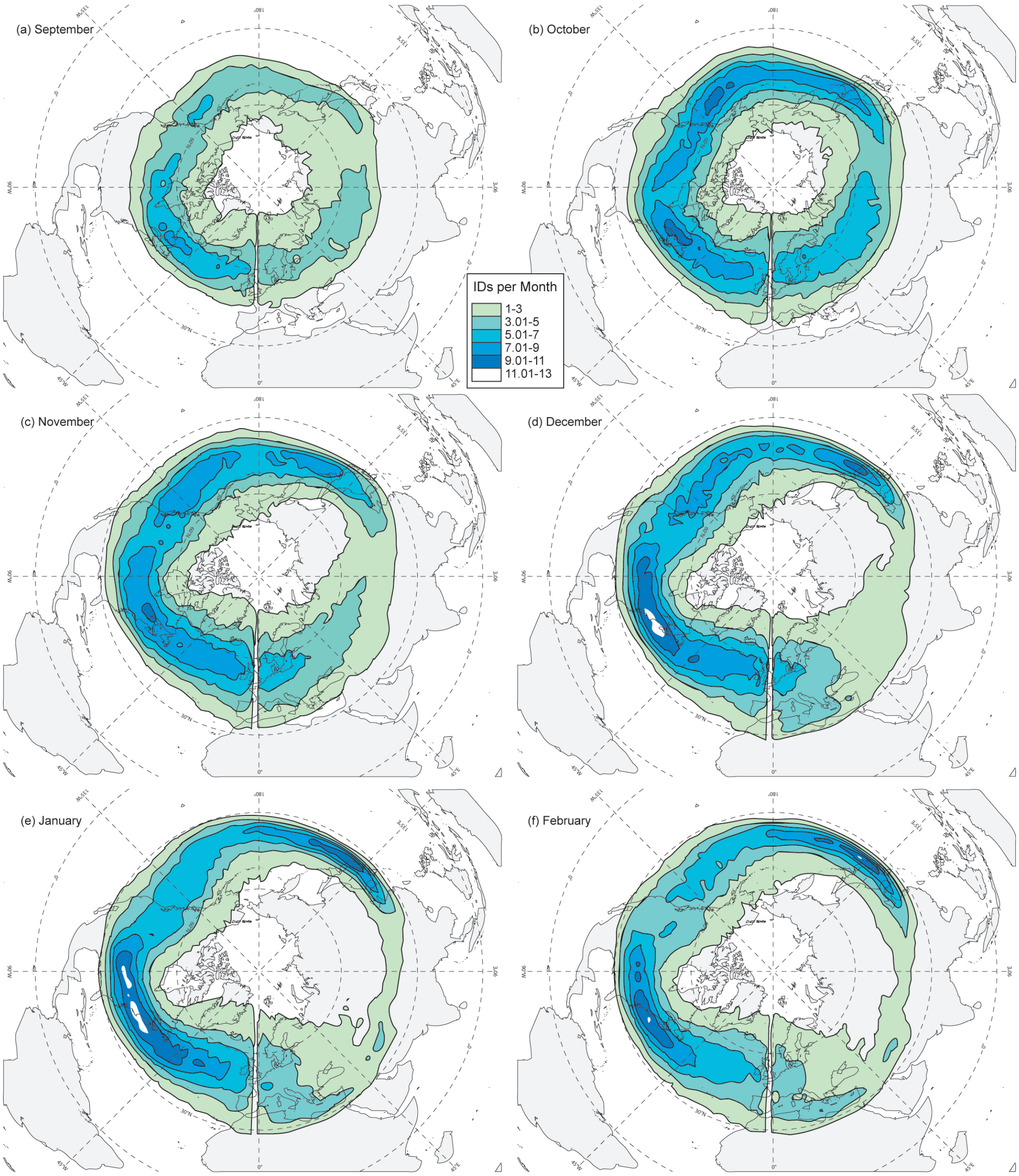


**Figure 3:** (a) Average frequency of Northern Hemisphere polar jet identifications during the month of September over the period 1960-2010. (b) As in Fig. 3a but for October. (c) As in Fig. 3a but for November. (d) As in Fig. 3a but for December. (e) As in Fig. 3a but for January. (f) As in Fig. 3a but for February.

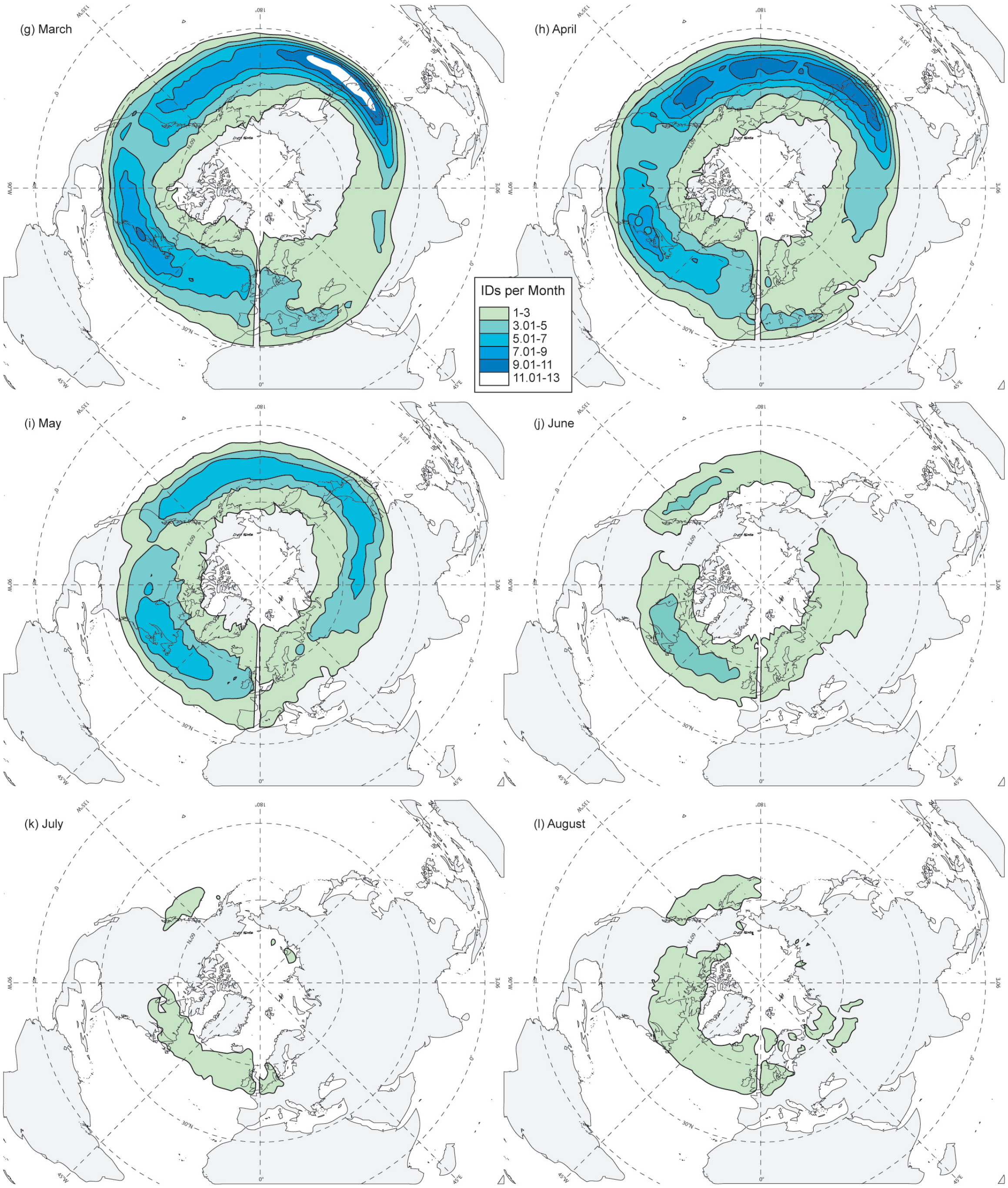


**Figure 3 (continued):** (g) As in Fig. 3a but for March. (h) As in Fig. 3a but for April. (i) As in Fig. 3a but for May. (j) As in Fig. 3a but for June. (k) As in Fig. 3a but for July. (l) As in Fig. 3a but for August.

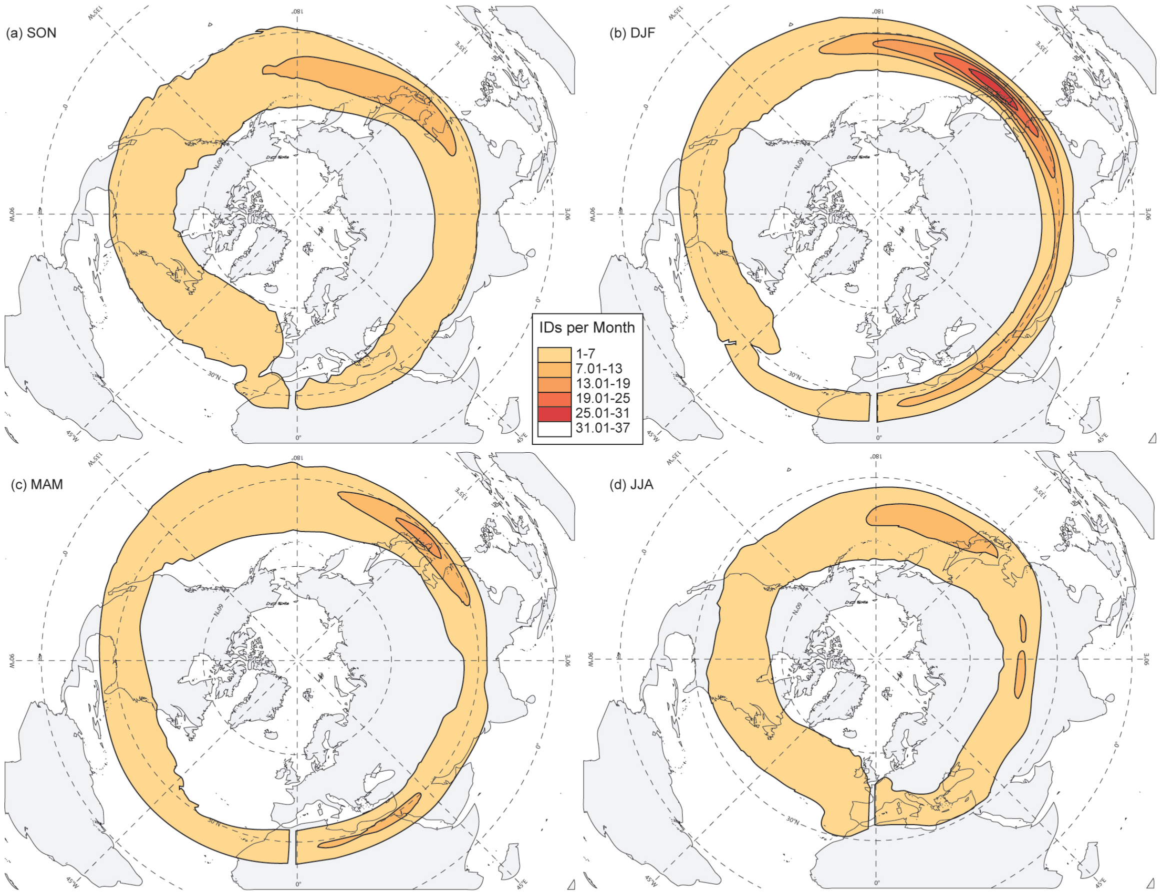


**Figure 4:** (a) Average frequency of Northern Hemisphere subtropical jet identifications during the three month period September-November over the period 1960-2010. (b) As in Fig. 4a but for the months of December-February. (c) As in Fig. 4a but for the months of March-May. (d) As in Fig. 4a but for the months of June-August.

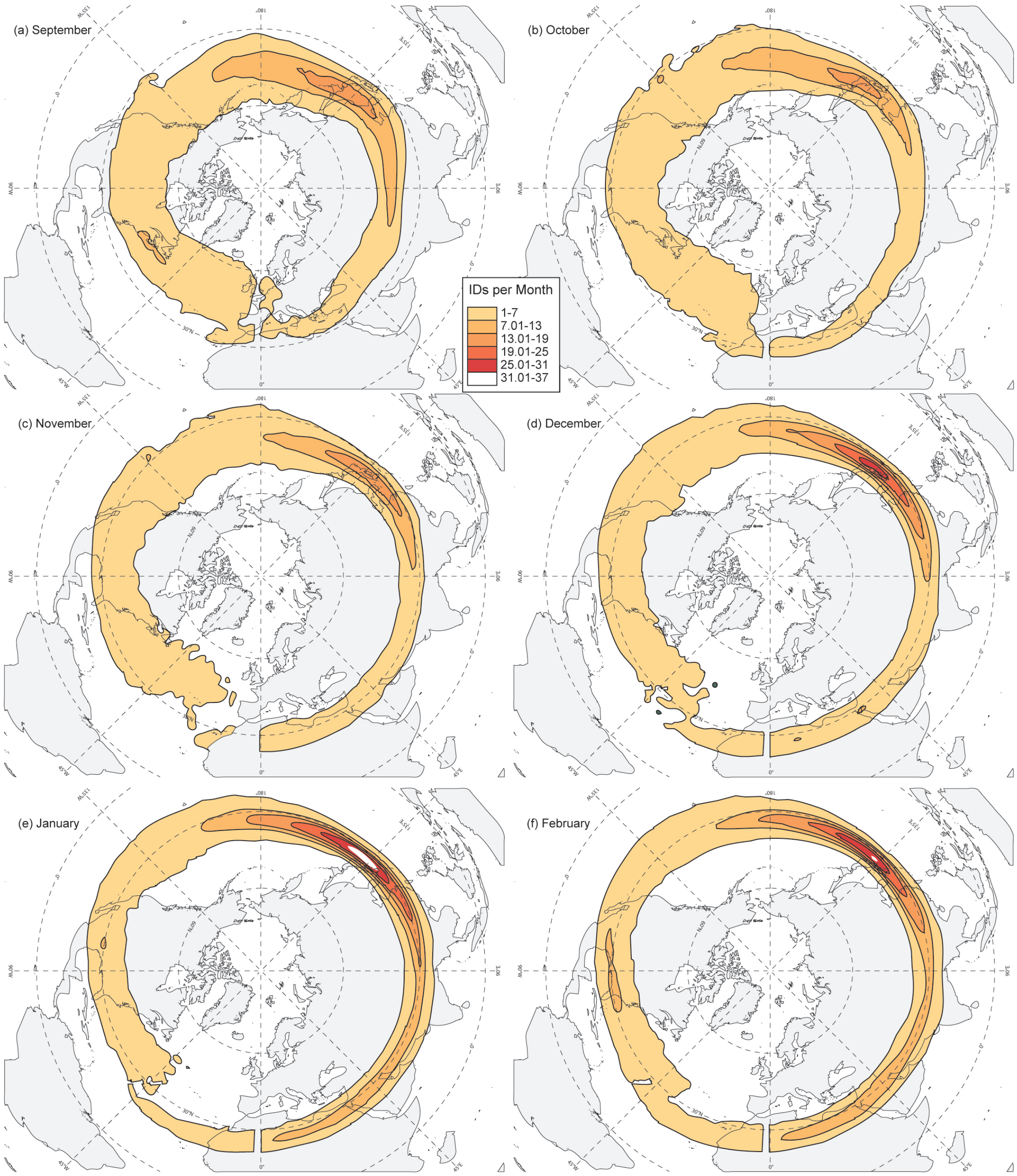


**Figure 5:** (a) Average frequency of Northern Hemisphere subtropical jet identifications during the month of September over the period 1960-2010. (b) As in Fig. 5a but for October. (c) As in Fig. 5a but for November. (d) As in Fig. 5a but for December. (e) As in Fig. 5a but for January. (f) As in Fig. 5a but for February.

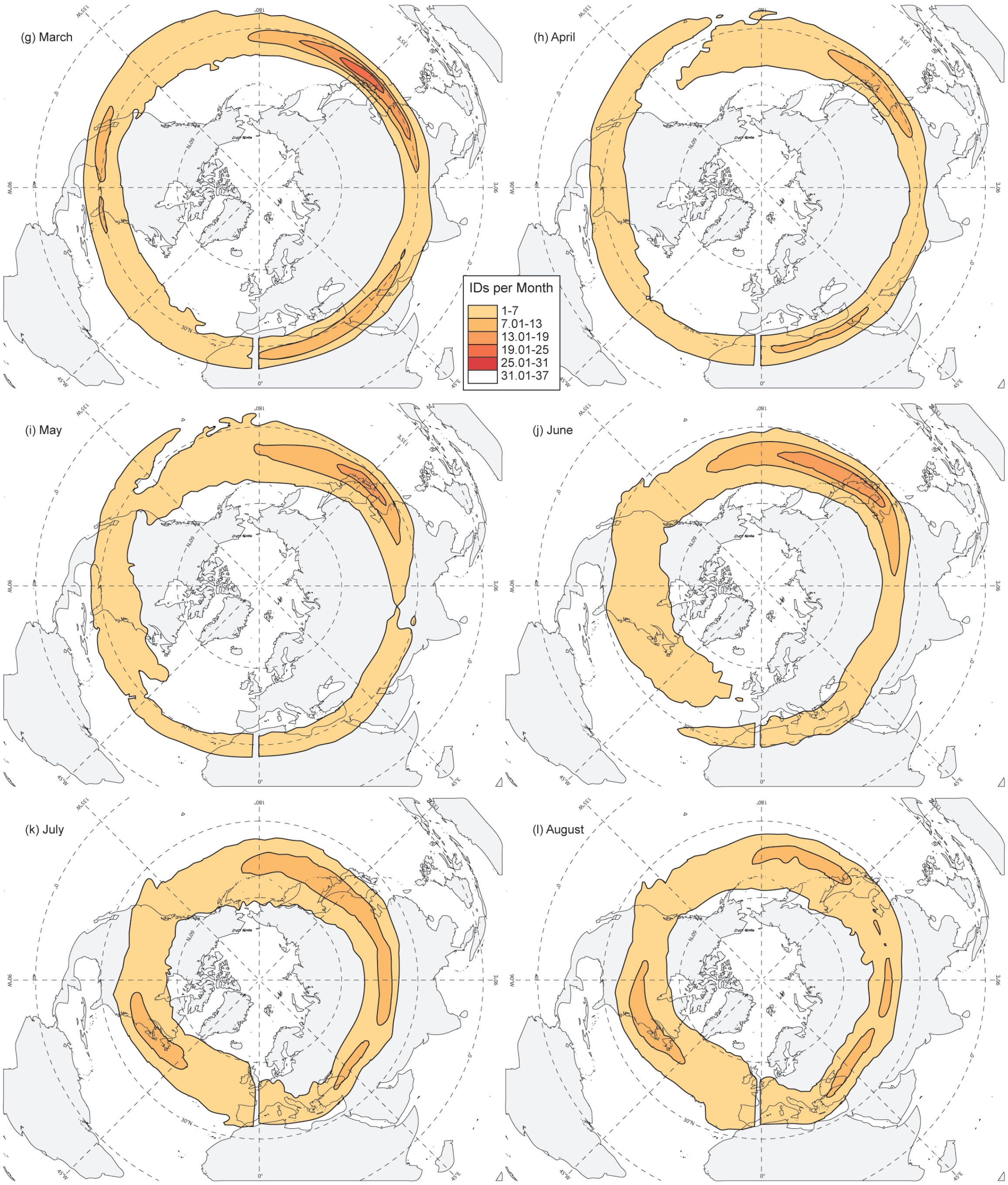


**Figure 5 (continued):** (g) As in Fig. 5a but for March. (h) As in Fig. 5a but for April. (i) As in Fig. 5a but for May. (j) As in Fig. 5a but for June. (k) As in Fig. 5a but for July. (l) As in Fig. 5a but for August.

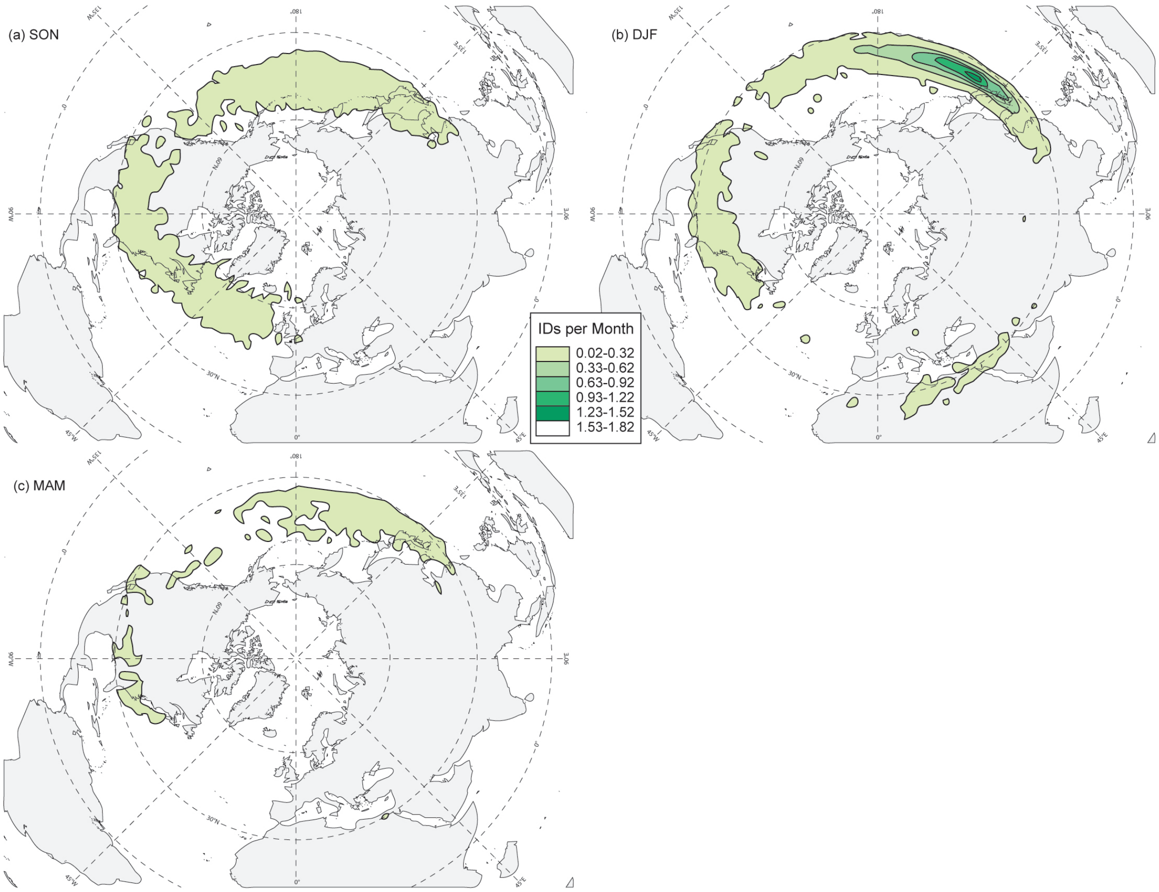


**Figure 6:** (a) Average frequency of Northern Hemisphere jet superpositions during the three month period September-November over the period 1960-2010. (b) As in Fig. 6a but for the months of December-February. (c) As in Fig. 6a but for the months of March-May.

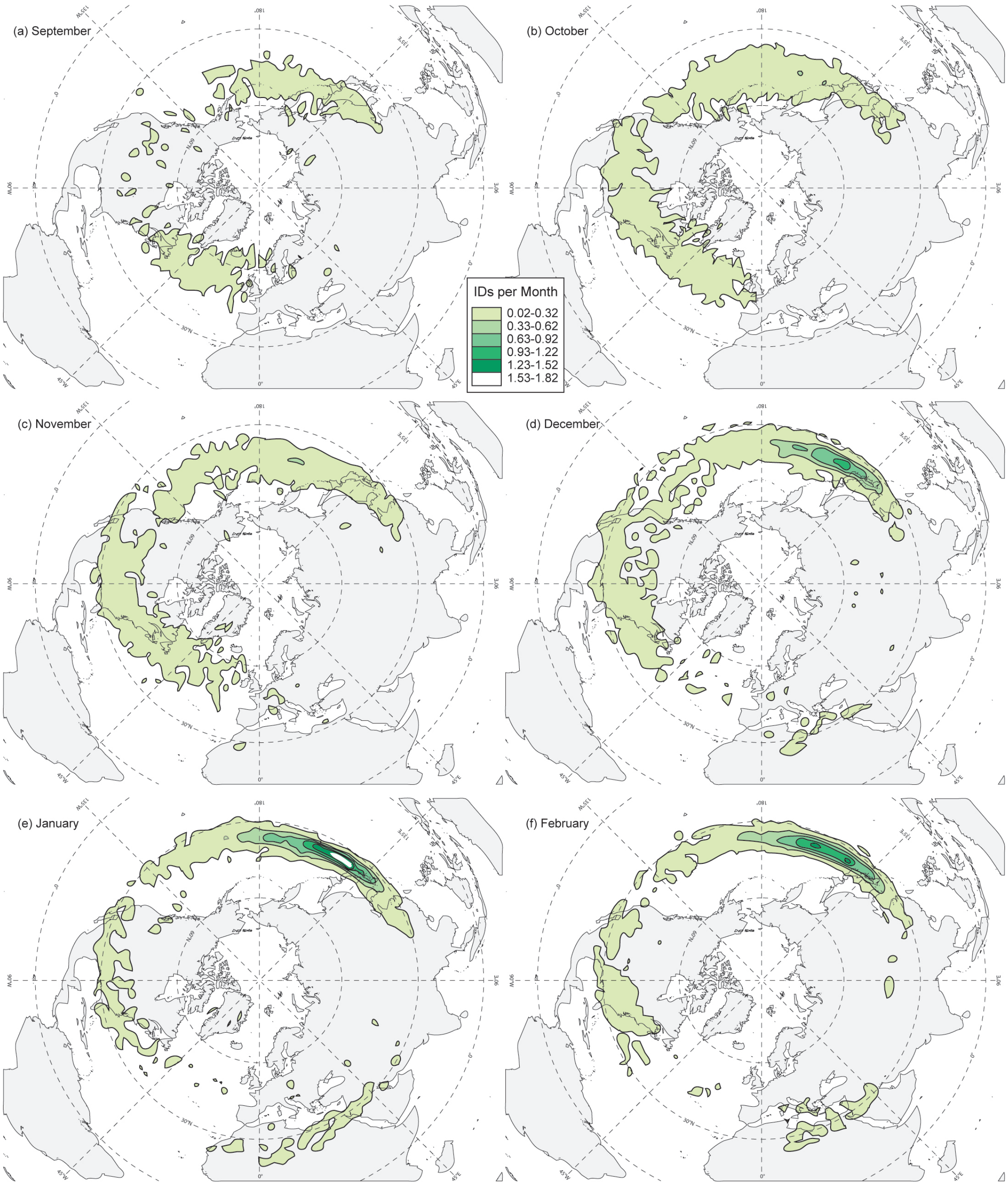


**Figure 7:** (a) Average frequency of Northern Hemisphere jet superpositions during the month of September over the period 1960-2010. (b) As in Fig. 7a but for October. (c) As in Fig. 7a but for November. (d) As in Fig. 7a but for December. (e) As in Fig. 7a but for January. (f) As in Fig. 7a but for February.

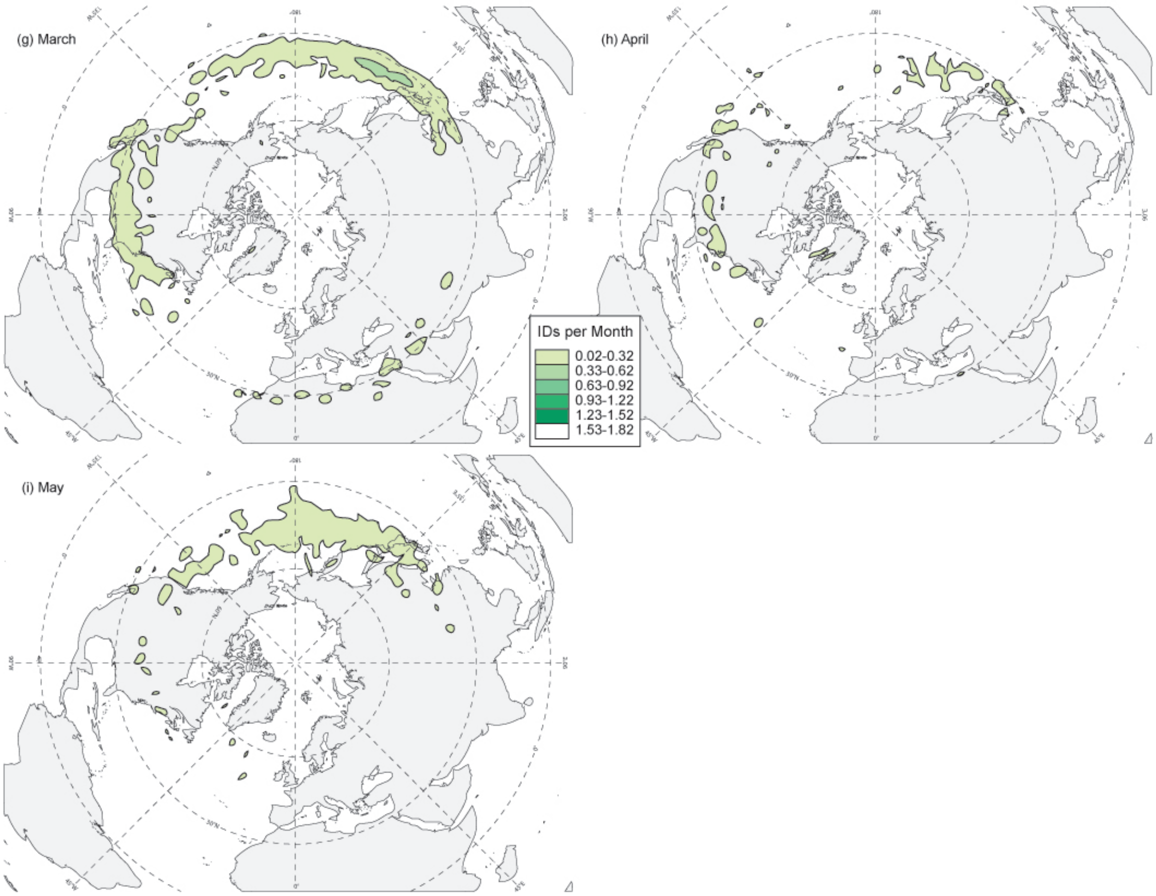


**Figure 7 (continued):** (g) As in Fig. 7a but for March. (h) As in Fig. 7a but for April. (i) As in Fig. 7a but for May.

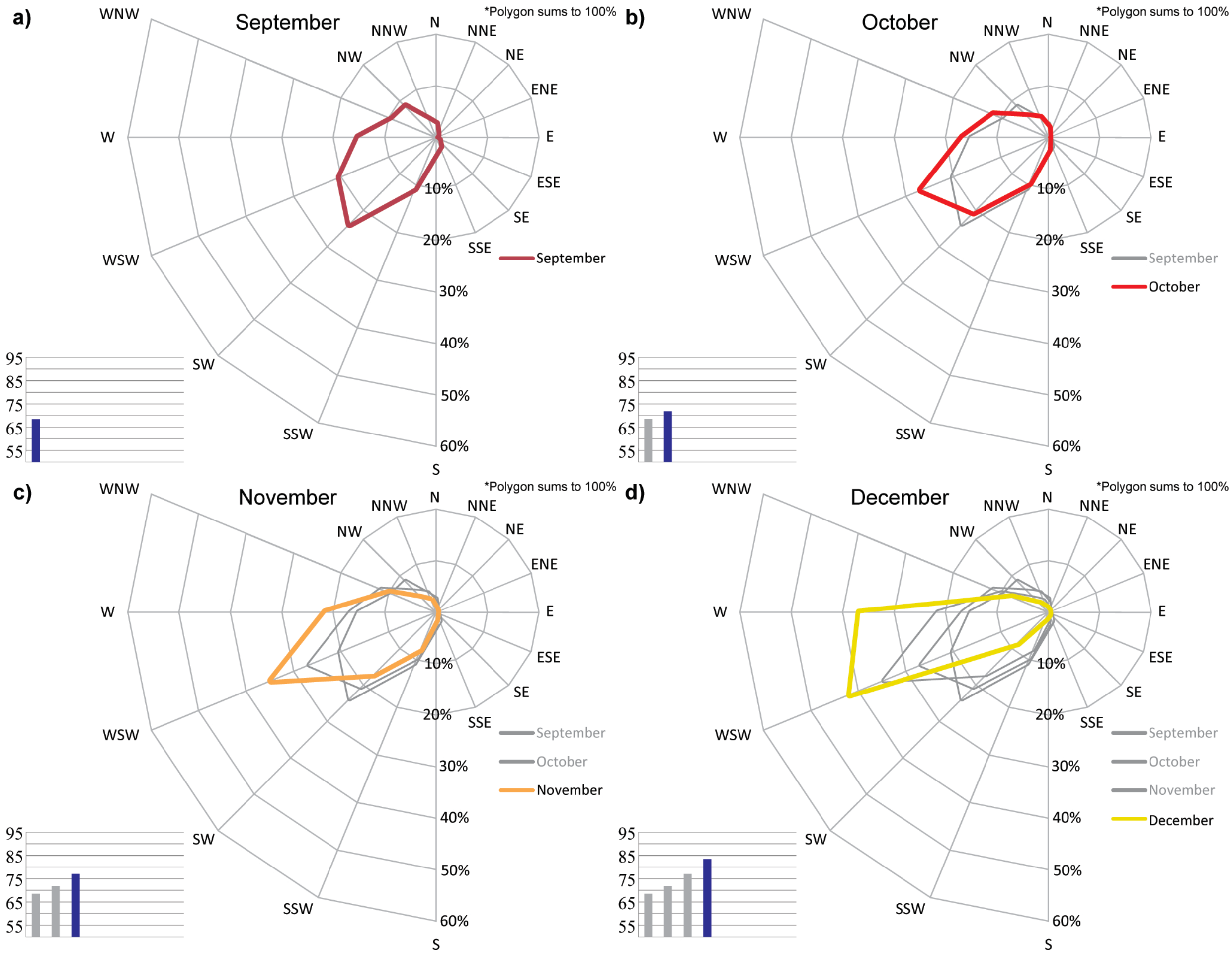


**Figure 8:** (a) Wind direction plotted on the wind rose for every Northern Hemisphere jet superposition identified during the month of September over the period 1960-2010. Average wind speed for each jet superposition in m s$^{-1}$ shown in blue on bar graph. (b) As in Fig. 8a but for but for October. (c) As in Fig. 8a but for but for November. (d) As in Fig. 8a but for but for December.

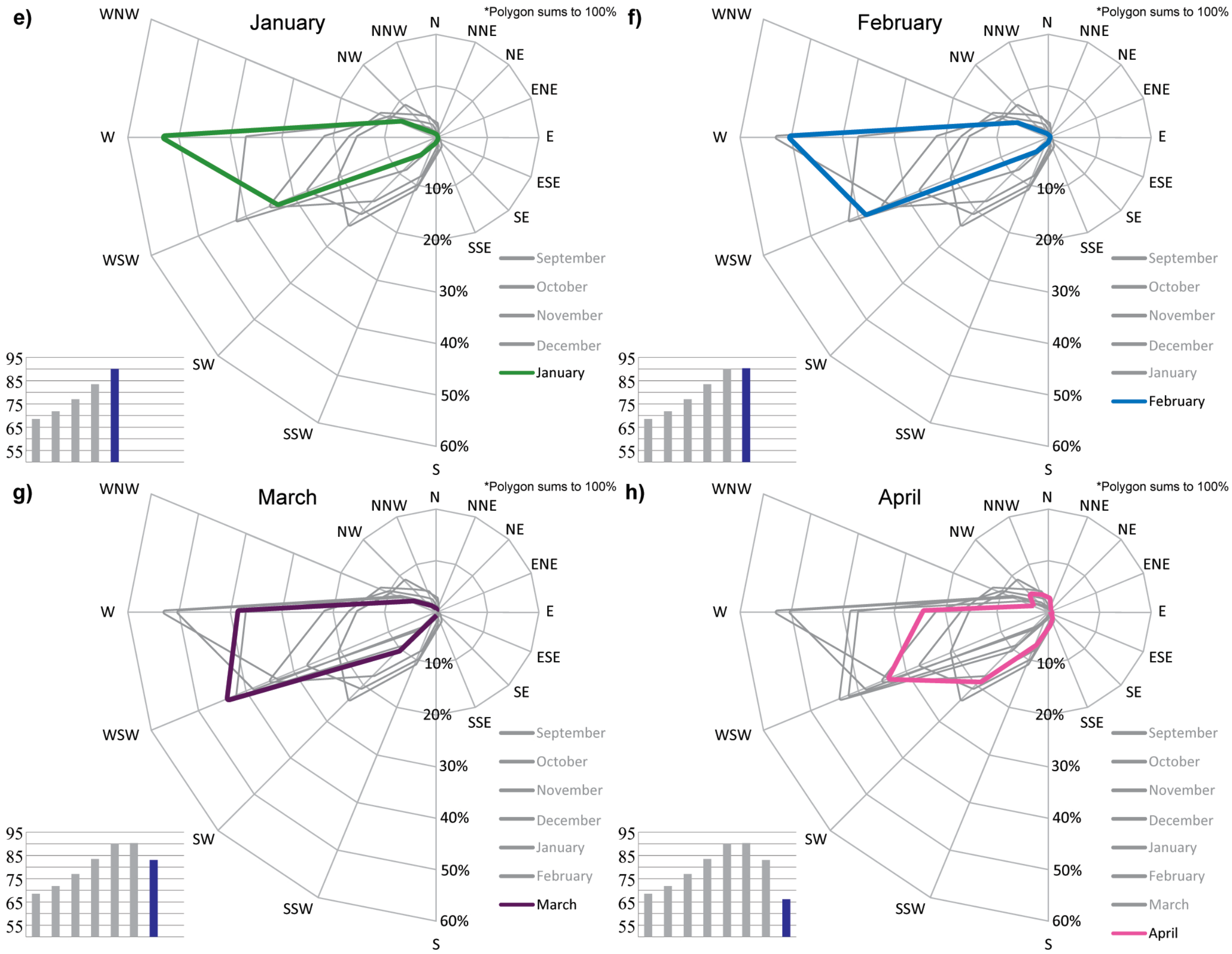


**Figure 8 (continued):** (e) As in Fig. 8a but for but for January. (f) As in Fig. 8a but for but for February. (g) As in Fig. 8a but for but for March. (h) As in Fig. 8a but for but for April.

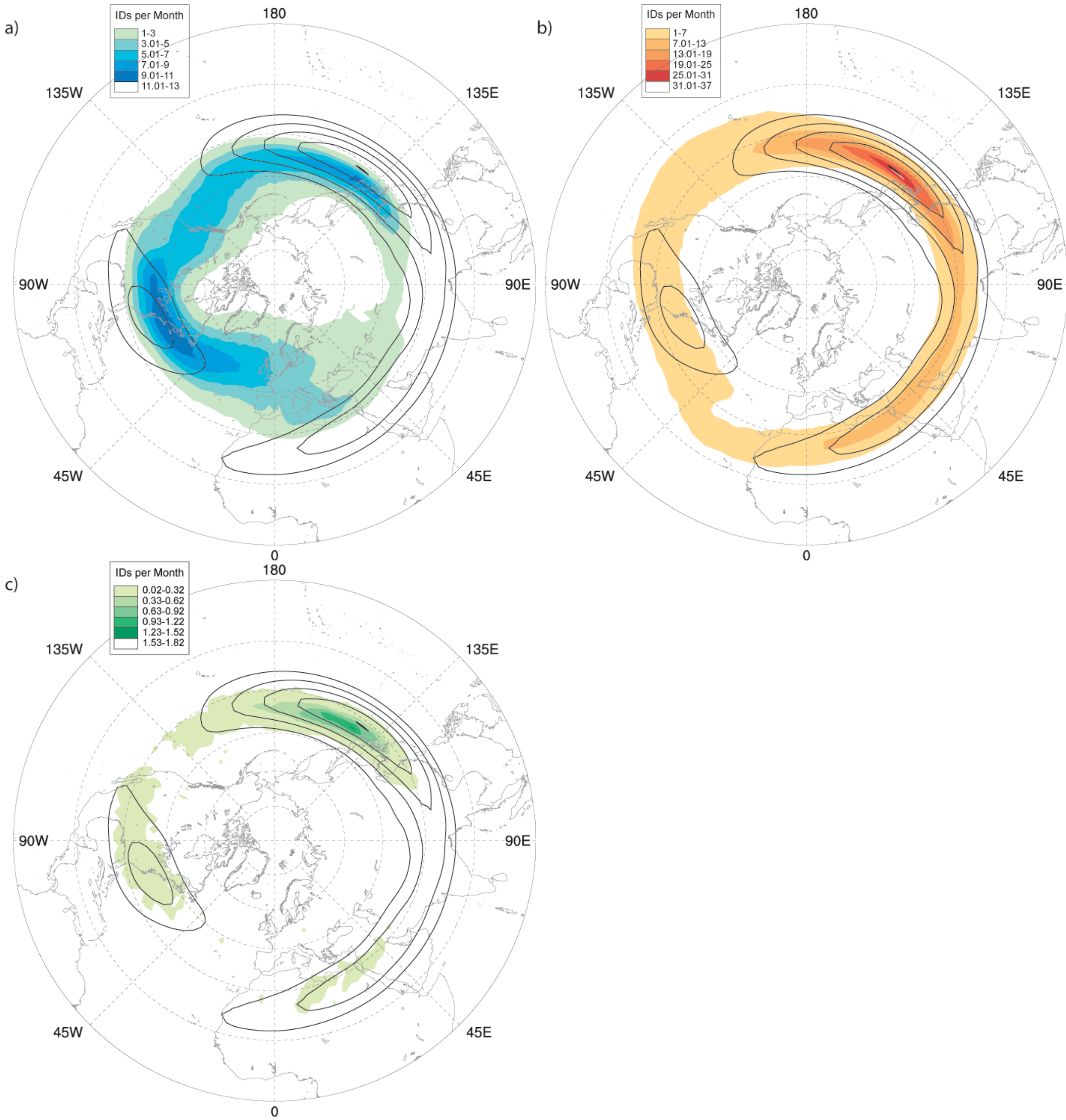


**Figure 9:** (a) DJF seasonal average frequency of polar jet identification (fill) and isotachs of average zonal (U-wind) at 250hPa (black contour) every 10 m $s^{-1}$ starting at 30 m $s^{-1}$ over the period 1960-2010. (b) As in Fig. 9a but with fill indicating subtropical jet identifications. (c) As in Fig. 9a but with fill indicating jet superposition identifications.

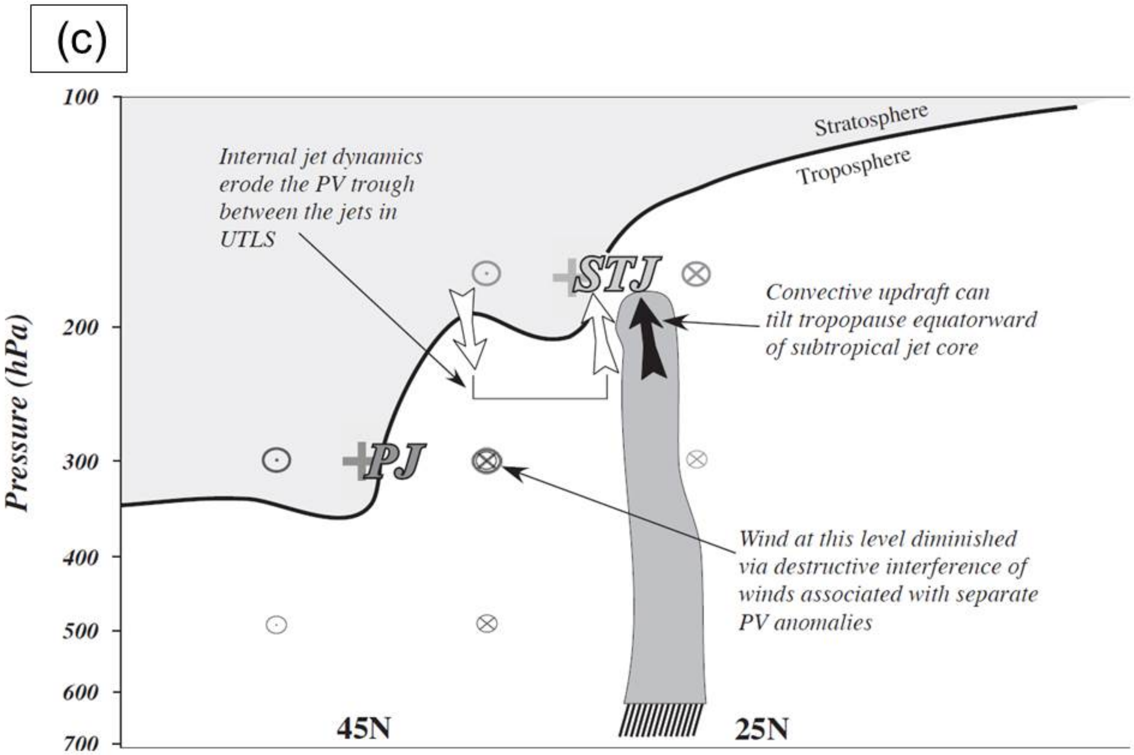


**Figure 10:** Schematic vertical cross section illustrating the dynamical processes that may Facilitate a superposition of the polar (PJ) and subtropical (STJ) jet. Each jet is associated with a tropopause level positive PV perturbation (signified by the + signs). Corresponding circulations at and below each perturbation are indicated by a circled x or ●. Solid black line is the 1.5 PVU isosurface with the lower stratosphere shaded gray. See text for explanation. (Adapted from Winters and Martin 2014).